Space-Borne Circular Antenna Array Optimization with Mountain Gazelle Optimizer for Element Failure Correction

Sunil Kumar[1], Dhiraj Kumar Singh[2], Avtar Singh[3], and Harbinder Singh[4]

[1]Department of Electrical, Electronics and Communication Engineering, Galgotias University, Greater Noida-201308, UP (India)
[2]School of Engineering and Technology, Amity University Haryana, Amity Education Valley, Gurugram, Manesar 122413, Haryana, India
[3]Shri Ram Murti Smarak College of Engineering & Technology, Uttar Pradesh, Bareilly, India
[4]Department of Electronics and Communication Engineering, UCRD, Chandigarh University, Mohali-140413, Punjab, India

Corresponding author: Harbinder Singh (e-mail: harbinder.ece@cumail.in; harvinder90@gmail.com).

ABSTRACT Active phase array antennas are capable of providing high gain, wider coverage, and dynamic beam switching in a desirable direction, thus making them extremely suitable for space-borne applications such as radio astronomy, satellite communication, deep space vehicles, telemetry tracking and control communication systems. Nonetheless, there is a probability that a single or multiple antenna elements go faulty in an array, because of which the radiation pattern of the array gets distorted. The distorted radiation pattern increases the side lobe level (SLL) and reduces the directivity and hence degrades the array performance. In such space applications where it is extremely tedious, time-consuming, and costly to replace the faulty elements, a self-recoverable mechanism of failure correction can be implemented by using metaheuristic algorithms, thus mitigating any manual intervention. The enhanced SLL not only wastes the radio frequency energy but also raises potential challenges due to interference caused by receiving and transmitting the signals in an undesirable direction. In this research article, a circular antenna array (CAA) is investigated for the element failure correction of a faulty array. A mechanism of a self-recoverable array is proposed, having the capability of restoring the SLL of a failed array by recalculating and reoptimizing the array parameters with the remaining active elements within the array. Radiation pattern recovery is achievable by implementing a metaheuristic known as the mountain gazelle optimizer (MGO), and its effectiveness is validated by comparing the simulated results with other algorithms.

INDEX TERMS Sidelobe level, array failure, mountain gazelle optimizer, array factor, radiation pattern

I. INTRODUCTION

ANTENNA arrays are crucial for improving the capacity and spectrum efficiency of wireless communication networks. Active phase antenna arrays are extensively used in satellite communication, television broadcasting, and radio astronomy, as well as adaptive beamforming services for signal and data collection [1]. A substantial number of radiating elements are frequently used in antenna array design, so there is always a potential that one or more of these components could malfunction. Failures of array structure elements in a system of antenna arrays can generate fast changes in field strength inside the array, which disturbs data acquisition due to the deformed radiation power pattern [2]. Degraded radiation patterns from faulty arrays caused by single or many element failures reduce the array's performance by raising SLL, reducing directivity, beam broadening, and significantly lowering gain. When compared to traditional single antennas, antenna arrays can generate a narrow beam with significantly better directivity and reduced SLL [3]. The circular antenna array (CAA), which is a planar geometrical structure with its elements grouped circularly, is widely used in communication applications because it has omnidirectional scanning capabilities and reliable beam patterns [4].

Since arrays are frequently utilized in many different fields, research into the correction of failed components of arrays is currently in progress. However, due to the complexity, expense, and time required to swap out a failed radiating component with a new element, failure correction mechanisms are still necessary for programs like space-borne communication [5]. Therefore, employing the array's remaining active elements, an investigation is being carried out regarding optimization-based far-field radiation pattern correction methods. In general, analytical methods for failed element problems with antenna arrays that are thought of as having non-uniform spacing are unproductive. This subject presents a difficult task for numerical techniques due to the arbitrary geometrical layout of the leftover non-defective

array members and the required beam form. Various algorithms are used to recover the faulty array, such as the genetic algorithm (GA) [6], firefly algorithm (FA) [7], artificial bee colony algorithm (ABC) [8], and particle swarm optimization (PSO) [9]. Nonetheless, these algorithms are implemented over different array configurations like linear and concentric circular arrays, but each one outperforms the others for different numbers of elements. Several authors investigated the correction of a non-uniform antenna array by readjusting the distance between radiating elements and excitation parameters. For space-based applications, it offers limitations, and it is not feasible to alter any distance physically [10]. To overcome this limitation, a non-uniform array is recovered by the amplitude and phase-only method by assigning zero weights to the faulty elements and reoptimizing the array with the remaining active elements [11]. In this research article a non-uniform CAA is synthesized with eight elements and faults are introduced at multiple locations of an array, the original SLL is recovered with the remaining active elements by implementing the MGO algorithms [12], and for its effectiveness, the simulated results are compared with spider wasp optimizer (SWO) [13] and zebra optimization algorithm (ZOA) [14].

II. Problem Formulation

A CAA is a planner array in which the radiating components are placed in a circular pattern configuration. CAA gives more coverage, reduced sensitivity, and more freedom in how radiating elements are placed [15]. In comparison to different configurations, CAA is also less prone to mutual coupling, making it appropriate for higher-dimensional applications [16]. Fig. 1 shows the geometrical layout of a CAA, which consists of (N) numbers of isotropic radiating antennas arranged in a circle with radius 'r' placed in the x-y plane. Given that all radiating substances have an isotropic nature and emit radiation uniformly in all directions. The array factor (AF) [17], which is calculated as follows in Eq. (1), can be used to explain the radiation pattern for this kind of geometrical configuration:

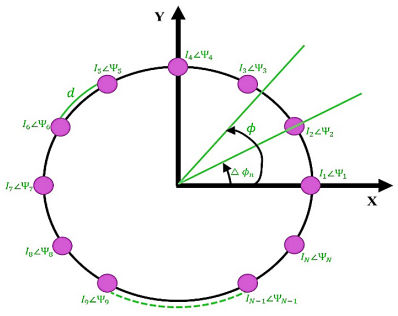

FIGURE 1. Geometrical configuration of CAA.

$$AF(\phi) = \sum_{n=1}^{N} I_n \, e^{j[\beta r cos(\phi - \phi_n) + \alpha_n]} \quad (1)$$

The angular position of the nth radiating element separated by distance d apart and placed in the x-y plane is described by ϕ_n as given by Eq. (2):

$$\phi_n = \frac{2\pi(n-1)}{N} \quad (2)$$

here wave number (β) is expressed in terms of N radiating antenna and spacing as in Eq. (3) [18].

$$\beta r = \frac{2\pi r}{\lambda} = \sum_{i=1}^{N} d_i = N d_\lambda \quad (3)$$

The orientation of the main lobe (ϕ_0) could be controlled by a phase regulating factor to provide the maximum value of the AF as given in Eq. (4):

$$\alpha_n = -\beta r cos(\phi_o - \phi_n) \quad (4)$$

Therefore, the AF can be expressed in the orientation of the main radiating lobe as in Eq. (5) [19]:

$$AF(\phi) = \sum_{n=1}^{N} I_n \, e^{j[\beta r(cos(\phi - \phi_n) - cos(\phi_o - \phi_n)) + \psi]} \quad (5)$$

The objective function (OF) is defined to recover the SLL in the desired direction of the main beam and an acceptable value of first null beam width (FNBW) with a good value of directivity as given in Eq. (6):

$$OF = |\emptyset_o - \emptyset_{des}| + \frac{|AF(\emptyset_{SLL} I, \beta, \emptyset_o)|}{|AF(\emptyset_{max} I, \beta, \emptyset_o)|} + |FNBW_O - FNBW_{DES}| \quad (6)$$

where the first segment in OF provides ϕ_o and ϕ_{des} that represents the orientation of the main lobe in the observed and desired direction, the second part evaluates the AF for the minimized value of SLL by removing any irregularities in the signal of interest, and the last segment provides the desired ($FNBW_{DES}$) and observed ($FNBW_O$) values of the FNBW. The weight factor (w) is associated with the OF, keeping in view that 'w' should remain zero for the faulty elements, and the OF is achieved by re-optimizing the remaining active elements in the array.

III. Mountain Gazelle Optimizer

A species of gazelle that inhabits the Arabian Peninsula and surrounding region is the mountain gazelle. Despite being widely dispersed, gazelles have a low population density. Strong territorial behavior is displayed by mountain gazelles, who create their territory far apart from one another. They create three different types of groups: flocks of young males, flocks of moms and young, and solitary males inside their territory. Battles between male gazelles happen frequently, and the struggle for resources is fiercer than the struggle for females. The social structure and environment of mountain gazelles serve as models for the MGO optimization method in mathematical modelling. It exhibits three different

elements of a dynamic group of gazelles, such as the behavior of maternity herds (MH), territorial and solitary males (TSM), bachelor male herds (BMH), and the pattern of migration in the search for foodstuff (MSF). These aspects are modeled mathematically and are represented as follows:

A. Territorial Solitary Male (TSM)

Mature male gazelles defend their territory from intruders, which is mathematically presented by Eq. (7) as:

$$TSM = male_{gazelle} - \left|\left(ri_1 \times BH - ri_2 \times X(t)\right) \times F\right| \times Cof_r \quad (7)$$

Such that ri_1 & ri_2 are two random integers of value either 1 or 2. The position vector of the best male gazelle is represented as malegazelle, and the value of different parameters is calculated by Eq. (8), (9), and (10) as:

$$BH = X_{ra} \times r_1 + M_{pr} \times r_2 \quad where\ ra = \left\{\frac{n}{3} \ldots . N\right\} \quad (8)$$

Here X_{ra} provides a random solution of young males in the range of ra, and M_{pr} is the average number of search agents, the number of gazelle is given as N, and r_1, r_2 are the two random numbers lying in the range of (0, 1).

$$F = N_1(D) \times exp\left(2 - iter \times \left(\frac{2}{Maxiter}\right)\right) \quad (9)$$

Where $N_1(D)$ represents random values with a size of problem dimension, and iter is the number of iterations.

$$Cof_i = \begin{Bmatrix} (a+1) + r_3, \\ a \times N_2(D), \\ r_4(D), \\ N_3(D) \times N_4(D)^2 \times \cos\left((r_4 \times 2) \times N_3(D)\right) \end{Bmatrix} \quad (10)$$

Where r_3 & r_4 are two random integers in the range of (0, 1) and $N_2(D)$, $N_3(D)$ and $N_4(D)$ are the randomly generated values. For every iteration, the value of a is calculated as given in Eq. (11):

$$a = -1 + Iter \times \left(\frac{-1}{MaxIter}\right) \quad (11)$$

B. Maternity Herd (MH)

The mother gazelle's behavior of safeguarding the offspring from predators can be represented in the mathematical form as given in Eq. (12):

$$MH = \left(BH + Cof_{1,r}\right) + \left(ri_3 \times male_{gazelle} - ri_4 \times X_{rand}\right) \times Cof_{1,r} \quad (12)$$

Such that X_{rand} depicts the vector position of the gazelle picked up randomly out of the population.

C. Bachelor Male Herds (BMH)

The Young, mature male gazelles establish their territories as part of their maturation phase and attempt to entice female gazelles to come along with them. Eq. (13) simulates this behavior as:

$$BMH = (X(t) - D) + \left(ri_5 \times male_{gazelle} - ri_6 \times BH\right) \times Cof_r \quad (13)$$

Such that ri_5 and ri_6 are the two random integers ranging from $(1, 2)$, $X(t)$ is the gazelle position vector for the current iteration. The value of D is determined from Eq. (14) as

$$D = \left(|X(t)| + \left|male_{gazelle}\right|\right) \times (2 \times r_6 - 1) \quad (14)$$

D. Migration in Search of Food (MSF)

Mountain gazelles use a roving foraging strategy to find their preferred green pasture. Eq. (15) models this random movement, where ub and lb denote the upper bound and lower search boundary, respectively, and r_7 is a random number ranging from (0, 1), and the pseudocode for implementing all the steps is depicted in Fig. 2.

$$MSF = (ub - lb) \times r_7 + lb \quad (15)$$

Inputs: iteration counter *(iter)*, maximum iteration *(MaxIter)*, population size *(N)*

Output: *gazelle's position*, and its *fitness value*

Initialize random gazelle populations, X_i *(i=1, 2... N)*

Evaluate the *fitness values of the population*

While *(Iter < MaxIter)*, **do**

  For *(every gazelle, X_i)* **do**

    Calculate **TSM** using equation (7)

    Calculate **MH** using equation (12)

    Calculate **BMH** using equation (13)

    Calculate **MSF** using equation (15)

  Evaluate the *fitness values* of TSM, MH, BMH, and MSF

  End for

Output best gazelle, X_{best} and its *fitness value*

End while

FIGURE 2. Pseudocode for implementing MGO

A graphical methodology illustrating the working and applicability of the CAA using the MGO is presented in Fig. 3. The radiation pattern of the CAA is controlled through the amplitude and phase excitation coefficients as defined in Eq. (5). The key performance parameters, including SLL, FNBW and main lobe alignment, are evaluated from the radiation pattern. The MGO algorithm is employed to estimate the optimal amplitude and phase coefficients for both fault-free and faulty conditions. To incorporate element failures, the amplitudes are multiplied by corresponding weights, where active elements are assigned unity weight and faulty elements are assigned zero. In the presence of faults, the radiation pattern is recovered using only the remaining active elements.

Initially, a population of candidate solutions representing amplitude and phase values is generated. The algorithm then updates these solutions using its internal mechanisms, namely MSF, BMH, MH and TSM as per Eq. (7) to (15), which operate in parallel to balance exploration and exploitation.

The updated solutions are evaluated using the objective function defined in Eq. (6) and the best solution (dominant gazelle) is selected for the next iteration. The population is iteratively updated and checked for convergence until the stopping criterion is satisfied. Finally, the optimized amplitude and phase coefficients are obtained, which are used to generate the restored radiation pattern with improved performance characteristics.

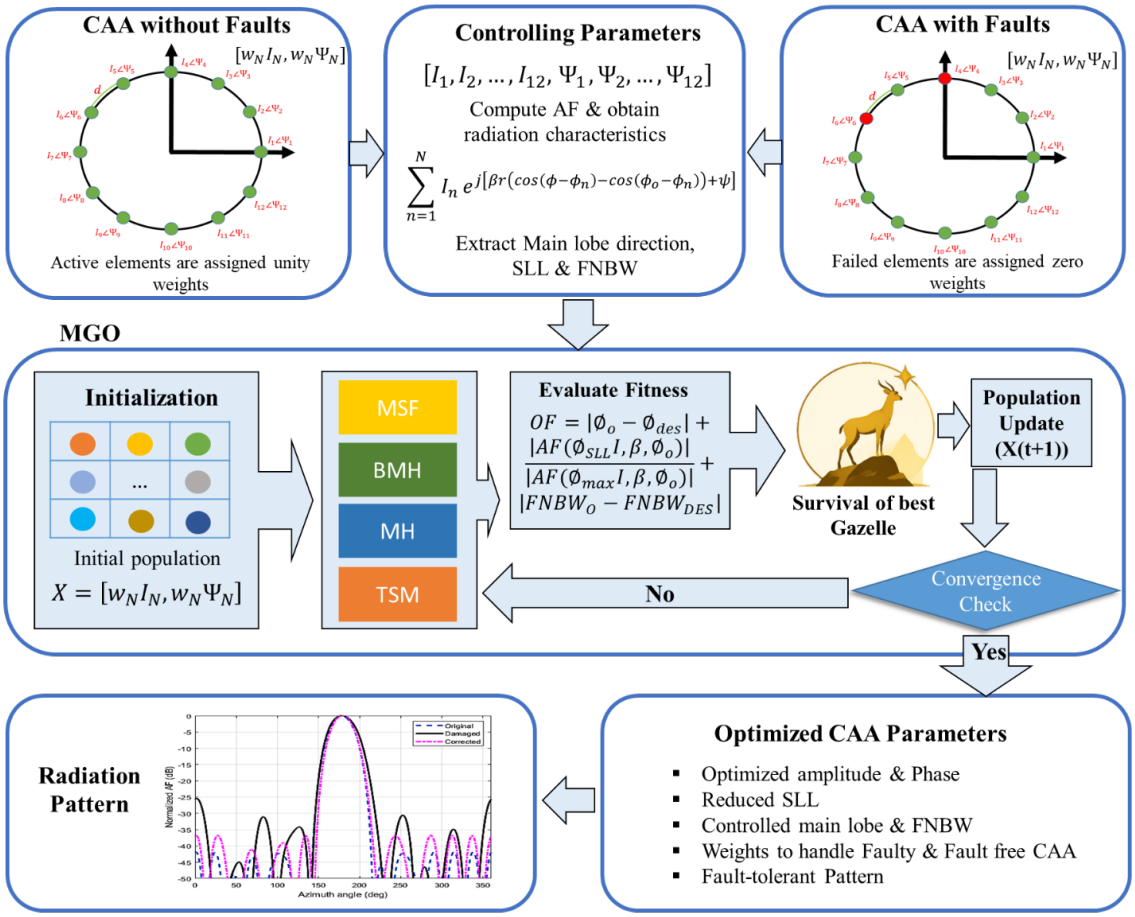

FIGURE 3. Graphical representation of the MGO based optimization process for CAA

IV. Simulation Results and Discussion

Consider a non-uniform CAA consisting of twelve elements, the position of faulty elements is introduced at the 4th and 6th positions. Here, the total number of parameters optimized is equal to twice the number of elements. The simulations are performed for 500 iterations on MATLAB 2021b with a Core i5 CPU to obtain the desired SLL from the remaining active elements. The simulated results show that MGO outperforms the other two algorithms, SWO and ZOA, and SLL of -41.67 dB, -37.96 dB, and -30.59 dB, respectively, is achieved, and the value of directivity obtained is 11.12, 12.68, and 12.52 dB, respectively, when there are no faulty elements as depicted in the convergence plot for the unfaulty array in Fig. 4.

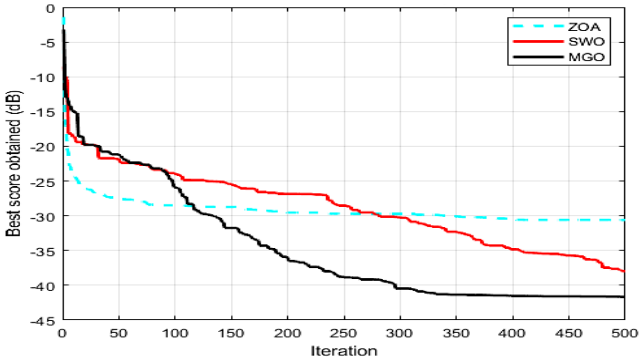

FIGURE 4. Convergence curve for twelve elements CAA without any faulty elements

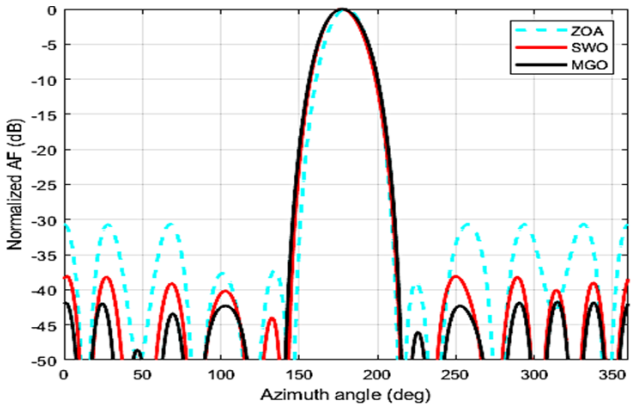

FIGURE 5. 2D radiation pattern without any fault in twelve elements CAA

The 2D radiation pattern without any faults with the main beam radiating at 180º is shown in Fig. 5. When a fault is introduced at a predefined location such as the 4th and 6th position, the radiation pattern deforms as depicted in Fig. 6. The CAA is now reoptimized by introducing zero weights to the faulty elements to ensure that their amplitude and phase remain zero. The correction of CAA is done by recovering the original radiation pattern by implementing MGO algorithms, and the results are compared with SWO and ZOA as depicted in Fig. 7. The performance comparison for twelve elements of CAA during recovery of SLL is presented in Table 1.

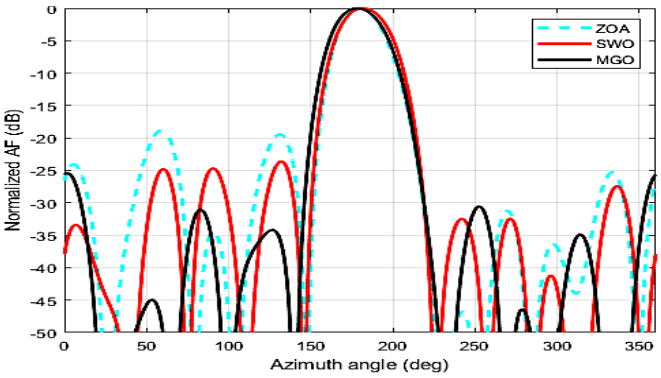

FIGURE 6. Deformed radiation pattern in faulty CAA with a faulty element at the 4th and 6th positions

It can be observed from the corrected pattern that the 2D radiation pattern distorted significantly in the presence of faulty elements, and thus the overall performance of the 12-element CAA degraded considerably. The recovery of the radiation pattern also depicts that the corrected value of SLL by using different algorithms, such as SWO, ZOA, and MGO, is -25.58 dB, -28.03 dB, and -36.71 dB, respectively, in comparison with their damaged SLL given by -23.96 dB, -19.86 dB, and -26.12 dB for SWO, ZOA, and MGO, respectively, which demonstrates the efficacy and efficiency of MGO in recovering the original radiation pattern from a faulty array. The outstanding performance in correcting the failure of a CAA by implementing MGO, along with providing an effective self-recoverable solution for practical real-life space applications. The recovery radiation pattern shows that MGO achieves nearly the same original radiation pattern even in the presence of faulty elements, as depicted in Fig. 8. The comparison of all three algorithms in correcting the faulty array is depicted in Fig. 9.

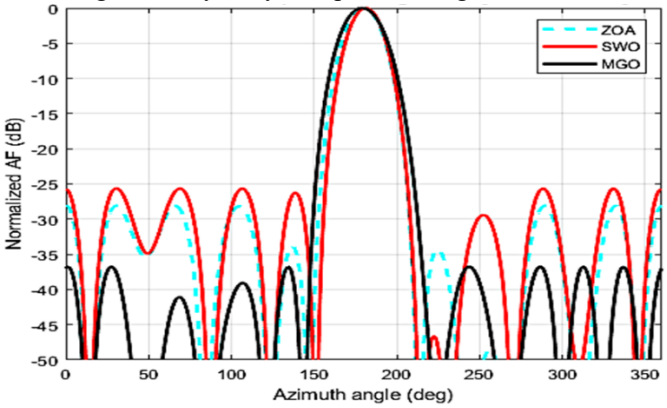

FIGURE 7. Correction of the radiation pattern for the twelve elements CAA with the remaining active elements

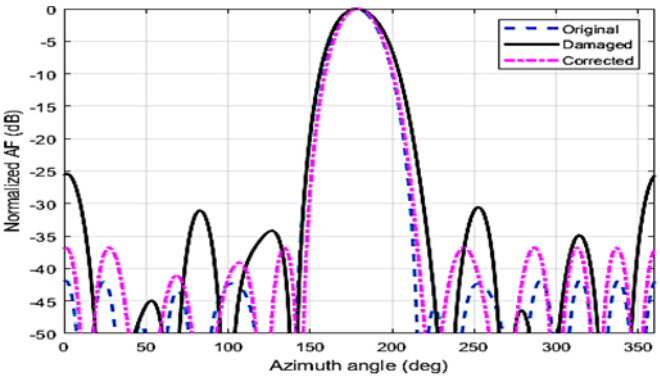

FIGURE 8. Corrected radiation pattern for twelve elements CAA by implementing MGO

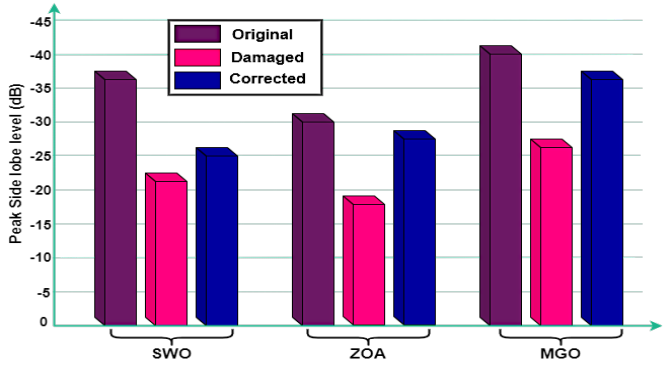

Figure 9. Performance comparison of different algorithms

The comparison of all three algorithms in correcting the faulty array is depicted in Fig. 8. The variation in the original SLL values among SWO, ZOA and MGO arises from the

independent convergence behaviour of each optimization algorithm under the same synthesis constraints. Since each method produces its own fault-free excitation distribution, the original SLL values are not necessarily identical.

For a more meaningful comparison of the fault-correction capability, the restoration gain from the damaged state to the corrected state is considered and is defined as:

$$Restoration\ Gain = |SLL_{corrected}| - |SLL_{damaged}|$$

where $SLL_{corrected}$ and $SLL_{damaged}$ denote the sidelobe levels of the corrected and damaged array patterns, respectively.

This parameter indicates the amount of sidelobe suppression recovered after applying the correction algorithm under the same failure condition. The calculated restoration gains are 1.62 dB for SWO, 8.17 dB for ZOA, and 10.59 dB for MGO. Among the reported algorithms, MGO provides the highest restoration gain, demonstrating its stronger capability to recover the radiation characteristics of the damaged array.

TABLE I. PERFORMANCE COMPARISON OF DIFFERENT ALGORITHMS FOR THE RECOVERY OF TWELVE ELEMENTS CAA

Algorithms	FNBW (degree)	CAA state	Peak SLL (dB)	Amplitude (In)	Phase (ψ)
SWO	57	Original	-37.96	0.6666, 0.7851, 0.3555, 0.5092, 0.5279, 0.5535, 0.6827, 0.6845, 0.3274, 0.8172, 0.2690, 0.5350	5.03, 9.05, 14.39, 123.98, -17.76, 21.77, 13.48, -0.22, -69.09, -21.09, 9.87, 4.70
		Damaged	-23.96	0.6666, 0.7851, 0.3555, 0, 0.5279, 0, 0.6827, 0.6845, 0.3274, 0.8172, 0.2690, 0.5350	5.03, 9.05, 14.39, 0, -17.76, 0, 13.48, -0.22, -69.09, -21.09, 9.87, 4.70
		Corrected	-25.58	0.5812, 0.7083, 0.5428, 0, 0.5916, 0, 0.6180, 0.6738, 0.5573, 0.4220, 0.8106, 0.5293	-46.49, 28.82, -29.61, 0, 8.41, 0, -6.40, 36.52, -4.67, -39.62, -110.97, 45.00
ZOA	61	Original	-30.59	0.6295, 0.5522, 0.2001, 0.3431, 0.2777, 0.3151, 0.2723, 0.3845, 0.2018, 0.2080, 0.3479, 0.2290	-16.49, -12.64, 8.07, 77.00, -72.10, 5.31, 1.06, -14.30, 2.75, 39.46, -50.90, 42.35
		Damaged	-19.86	0.6295, 0.5522, 0.2001, 0, 0.2777, 0, 0.2723, 0.3845, 0.2018, 0.2080, 0.3479, 0.2290	-16.49, -12.64, 8.07, 0, -72.10, 0, 1.06, -14.30, 2.75, 39.46, -50.90, 42.35
		Corrected	-28.03	0.7571, 0.2090, 0.2002, 0, 0.2280, 0, 0.2577, 0.3569, 0.2282, 0.2732, 0.2354, 0.6116	-7.28, 15.51, 23.74, 0, 9.11, 0, 40.98, 18.29, 44.67, 41.01, -3.04, -8.98
MGO	80	Original	-41.67	0.9988, 0.4593, 0.5114, 0.2000, 0.6998, 0.2000, 0.6594, 0.2348, 0.2001, 0.2000, 0.2000, 0.7887	-41.08, 21.14, -89.54, 18.17, 101.58, 27.08, 16.45, -36.52, 86.69, 92.71, 5.16, 29.99
		Damaged	-26.12	0.9988, 0.4593, 0.5114, 0, 0.6998, 0, 0.6594, 0.2348, 0.2001, 0.2000, 0.2000, 0.7887	-41.08, 21.14, -89.54, 0, 101.58, 0, 16.45, -36.52, 86.69, 92.71, 5.16, 29.99
		Corrected	-36.71	0.4289, 0.5639, 0.5801, 0, 0.6284, 0, 0.8206, 0.2037, 0.5917, 0.2967, 0.8908, 0.6516	132.54, -171.94, 45.19, 0, 51.13, 0, 178.96, 145.11, 149.56, -177.56, 133.12, 179.89

V. CONCLUSION

The radiation pattern of the CAA degraded significantly whenever there was a probability of malfunctioning in the array elements. The array's figure of merit considerably relies on the location and number of faulty elements present in the array. In case of fault occurrence for space-borne applications, it is extremely difficult, time-consuming, and costly to repair or replace a faulty element. The proposed concept of self-recoverable CAA is quite simple and cost-effective. In this proposed method of correcting faulty array, first of all, a 12-element CAA is synthesized for the best figure of merit, yielding SLL of -37.96 dB, -30.59 dB, and -41.67 dB for three different algorithms, namely SWO, ZOA, and MGO, respectively, with the corresponding value of FNBW being 57º, 61º, and 80º, respectively, depicting that the beam broadening is inversely proportional to SLL. The Synthesis results also validate it by the corresponding value of directivity as 12.68, 12.52, and 11.12 for SWO, ZOA, and MGO, respectively, which shows that directivity is poorer in the case of MGO. After these faulty elements are introduced at a predefined position of the 4th and 6th elements, the radiation pattern gets deformed, and SLL increases as -23.96 dB, -19.86 dB, and -26.12 dB for SWO, ZOA, and MGO, respectively.

An OF is proposed to recover the original patterns by assigning weight values equal to zero for all the faulty elements and ensuring the patterns are recovered with the remaining active elements. The corrected radiation pattern shows the excellent recovery capability of MGO when compared with different algorithms. The simulated results describe that the corrected SLL of -23.58 dB, -28.03 dB, and -36.71 dB for SWO, ZOA, and MGO, respectively can be achieved, validating the efficiency of MGO as best when compared with other algorithms. The proposed technique proves to be superior when it comes to recovering non-uniform CAA by reoptimizing the amplitude and phase of the remaining active elements, and it mitigates any possibility of human intervention in correcting the faulty array. The proposed technique could also be extended in the

future for the detection and correction of faults in a different geometrical layout of arrays.

The present results are obtained under ideal assumptions, including isotropic radiators and neglect of mutual coupling and hardware constraints. Incorporating practical element patterns and electromagnetic effects will be considered in future work to further validate the proposed fault-recovery approach for real active array systems.

REFERENCES

[1] K. Kundu, R. Bera, and N. N. Pathak, "Synthesis of Concentric Circular Antenna Array Using Whale Optimization Algorithm," IETE J. Res., Jul. 2022, doi: 10.1080/03772063.2022.2096703.

[2] S. U. Khan, I. M. Qureshi, F. Zaman, B. Shoaib, A. Naveed, and A. Basit, "Correction of faulty sensors in phased array radars using symmetrical sensor failure technique and cultural algorithm with differential evolution," Sci. World J., vol. 2014, 2014, doi: 10.1155/2014/852539.

[3] G. G. Roy, S. Das, P. Chakraborty, and P. N. Suganthan, "Design of non-uniform circular antenna arrays using a modified invasive weed optimization algorithm," IEEE Trans. Antennas Propag., vol. 59, no. 1, pp. 110–118, Jan. 2011, doi: 10.1109/TAP.2010.2090477.

[4] R. Bera, R. Lanjewar, D. Mandal, R. Kar, and S. P. Ghoshal, "Comparative study of circular and hexagonal antenna array synthesis using improved particle swarm optimization," in Procedia Computer Science, Jan. 2015, vol. 45, no. C, pp. 651–660, doi: 10.1016/j.procs.2015.03.126.

[5] L. Zheng, S. Yang, and Z. Nie, "Pattern synthesis with specified broad nulls in time-modulated circular antenna arrays," Electromagnetics, vol. 31, no. 5, pp. 355–367, Jul. 2011, doi: 10.1080/02726343.2011.579770.

[6] B. Artyushenko, "Genetic algorithm for antenna array with failed and deviated elements optimization," in 2007 4th IEEE Workshop on Intelligent Data Acquisition and Advanced Computing Systems: Technology and Applications, IDAACS, 2007, pp. 228–231, doi: 10.1109/IDAACS.2007.4488410.

[7] N. S. Grewal, M. Rattan, and M. S. Patterh, "A Non-Uniform Circular Antenna Array Failure Correction Using Firefly Algorithm," Wirel. Pers. Commun., vol. 97, no. 1, pp. 845–858, Nov. 2017, doi: 10.1007/s11277-017-4540-5.

[8] L. Wang, X. Zhang, and X. Zhang, "Antenna array design by artificial bee colony algorithm with similarity induced search method," IEEE Trans. Magn., vol. 55, no. 6, Jun. 2019, doi: 10.1109/TMAG.2019.2896921.

[9] H. A. Malhat, A. S. Zainud-Deen, M. Rihan, and M. M. Badway, "Elements Failure Detection and Radiation Pattern Correction for Time-Modulated Linear Antenna Arrays Using Particle Swarm Optimization," Wirel. Pers. Commun., vol. 125, no. 3, pp. 2055–2073, Aug. 2022, doi: 10.1007/s11277-022-09645-7.

[10] O. M. Bucci, A. Capozzoli, and G. D'Elia, "Diagnosis of array faults from far-field amplitude-only data," IEEE Trans. Antennas Propag., vol. 48, no. 5, pp. 647–652, May 2000, doi: 10.1109/8.855482.

[11] V. S. S. S. C. Vedula, S. R. C. Paladuga, and M. R. Prithvi, "Synthesis of Circular Array Antenna for Sidelobe Level and Aperture Size Control Using Flower Pollination Algorithm," Int. J. Antennas Propag., vol. 2015, 2015, doi: 10.1155/2015/819712.

[12] B. Abdollahzadeh, F. S. Gharehchopogh, N. Khodadadi, and S. Mirjalili, "Mountain Gazelle Optimizer: A new Nature-inspired Metaheuristic Algorithm for Global Optimization Problems," Advances in Engineering Software, vol. 174. Elsevier, p. 103282, Dec. 01, 2022, doi: 10.1016/j.advengsoft.2022.103282.

[13] M. Abdel-Basset, R. Mohamed, M. Jameel, and M. Abouhawwash, "Spider wasp optimizer: a novel meta-heuristic optimization algorithm," Artif. Intell. Rev., vol. 56, no. 10, pp. 11675–11738, Oct. 2023, doi: 10.1007/s10462-023-10446-y.

[14] E. Trojovska, M. Dehghani, and P. Trojovsky, "Zebra Optimization Algorithm: A New Bio-Inspired Optimization Algorithm for Solving Optimization Algorithm," IEEE Access, vol. 10, pp. 49445–49473, 2022, doi: 10.1109/ACCESS.2022.3172789.

[15] F. I. Tseng and D. K. Cheng, "Pattern Synthesis of Circular Arrays with Many Directive Elements," IEEE Trans. Antennas Propag., vol. 16, no. 6, pp. 758–759, 1968, doi: 10.1109/TAP.1968.1139293.

[16] A. E. Taser, K. Guney, and E. Kurt, "Circular antenna array synthesis using multiverse optimizer," Int. J. Antennas Propag., vol. 2020, 2020, doi: 10.1155/2020/3149826.

[17] K. Guney, A. Durmus, and S. Basbug, "Backtracking Search Optimization Algorithm for Synthesis of Concentric Circular Antenna Arrays," Int. J. Antennas Propag., vol. 2014, 2014, doi: 10.1155/2014/250841.

[18] M. Lin, Y. Gao, P. Liu, and J. Liu, "Theoretical Analyses and Design of Circular Array to Generate Orbital Angular Momentum," IEEE Trans. Antennas Propag., vol. 65, no. 7, pp. 3510–3519, Jul. 2017, doi: 10.1109/TAP.2017.2700160.

[19] A. Reyna, M. A. Panduro, D. H. Covarrubias, and A. Mendez, "Design of steerable concentric rings array for low side lobe level," Sci. Iran., vol. 19, no. 3, pp. 727–732, 2012, doi: 10.1016/j.scient.2011.08.028.